Research paper

Discovery of novel non-competitive inhibitors of mammalian neutral M1 aminopeptidase (APN)

Isel Pascual [a, *], Pedro A. Valiente [a], Gabriela García [a], Mario E. Valdés-Tresanco [a], Yarini Arrebola [a], Lisset Díaz [a], Lotfi Bounaadja [b], Rosa María Uribe [c], Mae Chappé Pacheco [d], Isabelle Florent [b], Jean-Louis Charli [c]

[a] Center for Protein Studies, Faculty of Biology, University of Havana, Cuba
[b] Molécules de Communication et Adaptation des Microorganismes, (MCAM, UMR 7245), Muséum National Histoire Naturelle, Sorbonne Universités, CNRS, CP 52, 57 Rue Cuvier, 75005, Paris, France
[c] Instituto de Biotecnología, Universidad Nacional Autónoma de México (UNAM), Ave Universidad 2001, Cuernavaca, Morelos, Mexico
[d] Instituto de Oncología y Radiobiología, Habana, Cuba

ARTICLE INFO

ABSTRACT

Neutral metallo-aminopeptidase (APN) catalyzes the cleavage of neutral and basic amino acids from the N-terminus of protein or peptide substrates. APN expression is dysregulated in inflammatory diseases as well as in several types of cancer. Therefore, inhibitors of APN may be effective against cancer and inflammation. By virtual screening and enzymatic assays, we identified three non-competitive inhibitors ($\alpha > 1$) of the porcine and human APN with K_i values in the μM range. These non-peptidic compounds lack the classical zinc-binding groups (ZBG) present in most of the APN inhibitors. Molecular docking simulations suggested the novel inhibitors suppress APN activity by an alternative mechanism to Zn coordination: they interacted with residues comprising the S1 and S5′ subsites of APN. Of note, these compounds also inhibited the porcine aminopeptidase A (pAPA) using a competitive inhibition mode. This indicated differences in the binding mode of these compounds with APN and APA. Based on sequence and structural analyses, we predicted the significance of targeting human APN residues: Ala-351, Arg-442, Ala-474, Phe-896 and Asn-900 for improving the selectivity of the identified compounds. Remarkably, the intraperitoneal injection of compounds BTB07018 and JFD00064 inhibited APN activity in rat brain, liver and kidney indicating good bio-distribution of these inhibitors in vivo. These data reinforce the idea of designing novel APN inhibitors based on lead compounds without ZBG.

© 2017 Elsevier B.V. and Société Française de Biochimie et Biologie Moléculaire (SFBBM). All rights reserved.

1. Introduction

Mammalian neutral aminopeptidase (APN) plays pivotal roles in many physiological processes, such as pain sensation, blood pressure regulation, tumor angiogenesis and metastasis, immune cell chemotaxis, sperm motility, cell-cell adhesion, and coronavirus entry [1]. Accordingly, APN is a major target for treatment of diseases related to these physiological processes [1]. APN is the most extensively studied member of the M1-family of zinc-dependent aminopeptidases [1]. This enzyme is widely expressed on cell surfaces of tissues, such as intestinal epithelia and the nervous system [1]. APN is a type II membrane protein generally found as a homodimer in several mammalian species. Full-length human APN consists of 967 amino acids with a short N-terminal cytoplasmic domain, a single transmembrane segment, and a large ectodomain containing two catalytic motifs highly conserved across the M1 family: the zinc-binding motif HEXXHX18E and the exopeptidase signature GXMEN [2].

The general catalytic mechanism of mammalian APN is believed to be similar to that of prototypic zinc peptidase thermolysin,

which involves catalytic water attacking scissile peptide bonds [3]. However, the means by which substrates gain access to the catalytic site and how products are released have been the subject of some debate for several members of the M1 family [4–6]. APN preferentially cleaves neutral amino acids, most notably alanine, off the N terminus of peptide substrates leading to their activation/inactivation in the extracellular space. Mammalian APN operates ubiquitously in peptide metabolism pathways. It plays important roles in pain sensation and mood regulation by catalyzing the metabolism of neuropeptides that process sensory information. One of these neuropeptides is enkephalin, which binds to opioid receptors and has pain-relief and mood-regulating effects [7]; APN hydrolyses and shortens the *in vivo* life of enkephalin. APN is moreover involved in blood pressure regulation; it degrades the vasoconstrictive peptide angiotensin-III, causing vasodilation and lowered blood pressure [8]. An endogenous APN inhibitor, substance P, blocks both the enkephalin-dependent and angiotensin-dependent pathways [9,10]. APN is also overexpressed on the cell surface of almost all major cancer forms and is essential for tumor angiogenesis by degrading angiogenic peptides [11]. A natural APN inhibitor, bestatin, is a substrate analog for APN and demonstrates antitumor activities [12]. However, it should be noted that these generic inhibitors often show activity against other aminopeptidase families [13].

The resolution of the three-dimensional structures (3D) of human APN in complex with angiotensin-IV and two peptidomimetic inhibitors, amastatin and bestatin [2], allows the application of structure-based drug discovery approaches to screen novel inhibitors. In this study, we identified three non-competitive inhibitors of the human and porcine APN by combining virtual screening and enzymatic assays. These non-peptide inhibitors lack the typical zinc-binding groups (ZBG) present in most of the APN inhibitors. Molecular docking simulations suggested these compounds hindered APN activity by an alternative mechanism to Zn coordination. Notably, the intraperitoneal injection of compounds BTB07018 and JFD00064 inhibited APN activity in rat brain, liver and kidney indicating a good bio-distribution.

2. Material and methods

2.1. Materials

Porcine kidneys were kindly donated by the Porcine Research Institute, Cuba; human placenta free of viruses and germs from the Center of Placental Histotherapy and the Institute of Oncology and Radiobiology, Cuba. DEAE Sephacel and Sephadex G200 were purchased from Amersham Biosciences, L-Leu-AMC and bestatin from Sigma-Aldrich, and L-Leu-pNA from Bachem. The inhibitors identified by virtual screening in the Hitfinder database were purchased from Maybridge, UK. Other reagents used were of analytical grade. The ^{1}H NMR data of the identified inhibitors supplied by the provider are included in Supplementary Information Fig. 1.

2.2. Virtual screening

The bidimensional structures of 14400 compounds of the Maybridge HitFinder Library were downloaded in the Structure Data File (SDF) format. The building of 3D structures, and conversion to PDBQT format were performed with the Open Babel software [14]. Docking simulations were conducted with the Autodock4$_{Zn}$ force field [15] implemented in the Autodock4 software [16] using as target the 3D structure of the hAPN:amastatin complex [2] (PDB code: 4FTY). The ten poses generated for each compound and the L-Leu-pNA substrate were ranked using the Autodock$_{ZN}$ force field [15]. The four best-ranked compounds based

on the binding energy with the hAPN were filtered using the PAINS-Remover web server (http://cbligand.org/PAINS) to exclude Pan Assay Interference Compounds [17]. Three-dimensional representations of the interactions of the best ranked pose of each hAPN:inhibitor complex were obtained using default parameters of the LIGPLOT software [18]. The 3D structures of the APN-inhibitor-substrate complexes were generated by superimposing the 3D structure of the APN-substrate and APN-inhibitor complexes using the salign routine [19] implemented in the Modeller software [20].

2.3. Sequence analysis

We analyzed five mammalian amino acid sequences homologous to human APN (AMPN_HUMAN), AMPN_PIG (Pig), AMPN_RAT (Rat), AMPN_BOVINE (Bovine), AMPN_MOUSE (Mouse). Pig, rabbit, rat and bovine sequences share 76.3 to 79.8% sequence identity (ID) with human APN. We also included in our analysis two human acid aminopeptidases of the M1 family: the glutamyl aminopeptidase (AMPE_Human, 34.7% ID) and the endoplasmic reticulum aminopeptidase (ERAP1_HUMAN, 33.1% ID). The multiple sequence alignment of mammalian aminopeptidases was performed using the Clustal W software [21]. The multiple alignments were manually parsed by analyzing the gaps, conserved amino acid regions and the secondary structure information using Seaview software [22].

2.4. Aminopeptidase N and aminopeptidase A preparations from human placenta and porcine kidney cortex

Microsomes containing hAPN were prepared from human placenta; placenta was cut with scissor and homogenized in 50 mM Tris-HCl pH 8 (buffer A; 2:1 mL/g) with a Waring blender (3 × 10 min, 4 °C). The crude extract was centrifuged at 3000 g, 4 °C during 15 min. The supernatant was centrifuged at 10 000 g at 4 °C for one hour. The microsomal fraction in the sediment was washed twice with 50 mM Tris-HCl pH 8, 1 M NaCl, and centrifuged as above, before final resuspension in 50 mM Tris-HCl pH 8, 0.1% of Triton X100 (Buffer B) for use in enzyme activity assays.

Porcine kidney APN (pAPN) was partially purified from porcine kidney cortex. Briefly, kidney cortex was dissected from fresh or recently thawed porcine kidneys, washed with cold distilled water, weighted, cut in small pieces with scissors and homogenized in distilled water (2 mL/g). The homogenate (crude extract) was treated with 0.1% Triton X100 to solubilize membrane-bound proteins, and centrifuged (10 000 g for 1 h at 4 °C). The supernatant was extensively dialyzed using dialysis membranes with a 10 000 Da cut off (Spectrapor) vs Buffer B. The dialyzed sample was applied to a DEAE-Sephacel column (12 × 1.6 cm) equilibrated with buffer B; the column was washed and retained components eluted stepwise, using increasing NaCl concentrations (from 0.15 to 1.0 M) in buffer B. The linear flow rate was 29.9 cm/h. The active fractions were concentrated by ultrafiltration and applied on a Sephadex G200 column (86 × 1.5 cm) equilibrated in buffer B; the linear flow rate was 6.81 cm/h. The active fractions were concentrated by ultrafiltration and stored until used for APN activity. The enzyme was partially purified 32 fold, with a 73% yield, and a final specific activity of 0.28 U/mg (Supplementary Information Fig. 2).

Microsomal porcine kidney cortex glutamyl aminopeptidase (porcine aminopeptidase A; pAPA) was prepared as described for human APN.

2.5. Monitoring of human, rat and porcine aminopeptidase activities

Soluble porcine kidney APN activity (0.02 mg/mL) was

measured as described by Tieku and Hooper [23] using the substrate L-Leu-pNA in buffer B and 1 mL of final volume assay. The release of *p*-nitroaniline was measured every 15 s during 5 min at 405 nm, at 37 °C using a Genesys 10 UV kinetic spectrometer (Thermo Electron Corporation, USA). pAPA activity (1 mg/mL of microsomes) was measured using buffer B, 1 mM $CaCl_2$, using the substrate L-Glu-pNA, as for pAPN.

For *in vivo* experiments, the evaluation of rat APN activity in microsomal preparations was performed in similar kinetic assay conditions, with 30 min assay time, 0.3 mL volume assay, a 96 wells plate reader Multiskan EX (Thermo Electron Corporation, Shangai), and the software "Reaction Kinetic".

Human placental aminopeptidase N activity (0.25 mg/mL of microsomes) was measured using L-Leu-AMC as a substrate in buffer B in a final assay volume of 200 μL. The kinetic assays were run at 37 °C during 40 min in 96 wells plates, and the AMC fluorescence was measured at 460 nm (bandwidth: 40) upon excitation at 360 nm (bandwidth: 40) in a BioTek FL600 fluoromark spectrofluorometer [24,25].

2.6. In vitro inhibition studies

The inhibitors were prepared as a stock solution of 10 mM in DMSO and diluted in buffer B to obtain the desired range of concentrations. To rule out an interference of the inhibitors with the activity assays, their absorbance at 405 nm and emission spectra upon excitation at 360 nm were determined. The inhibitors did not produce interference in the assays (Supplementary Information Fig. 3). The effects of the inhibitors were determined by quantifying the decrease of pAPN or hAPN activity in aliquots pre-incubated with the inhibitor (0.3–30 μM) for 30 min at 37 °C (n = 4) as proposed by Copeland (2000) [26]. In parallel, the effect of bestatin (0.02–300 μM) was assayed in similar conditions (n = 4). The IC_{50} value was determined by nonlinear regression of all the data from the dose-response curve using the software GRAFIT 6.0. Substrate concentration in the inhibitory assays was equal or lower than one K_M value to avoid competition between substrate and inhibitor. The K_M values were determined by adjusting the experimental data of initial rate at increasing substrate concentrations (pAPN: 0.06–7.5 mmol/L L-Leu-pNA; hAPN: 0.01–0.8 mmol/L L-Leu-AMC) to the Michaelis-Menten hyperbole model (n = 3) [26]. A similar procedure was followed to evaluate the effect of the inhibitors on pAPA activity, as a preliminary study of selectivity inside the M1 family.

To discard denaturing effects of the inhibitors on APN, we tested the reversibility of inhibitor-enzyme binding by a dilution study adapted from the procedure proposed by Copeland (2013) [27]. pAPN, at a concentration of 10-fold over the concentration required for the activity assay, was incubated with a fixed concentration of each inhibitor (3 μM) during 30 min. Substrate (at a concentration equivalent to 1 K_M value) in buffer B was then added to generate a rapid 10-fold dilution of the enzyme-inhibitor mixture to initiate the reaction. In parallel, a control assay included the enzyme submitted to similar conditions of dilution, but without an inhibitor.

Once the reversibility of the system was established, to study the kinetic mechanism of classical reversible inhibition vs hAPN and pAPN, enzyme assays were conducted at increasing substrate concentration (0.15–1.8 mM of L-Leu-pNA for pAPN, 0.03–0.3 mM of L-Leu-AMC for hAPN) in the presence of 0.5–10 μM of Maybridge compounds or 1–50 μM of bestatin (n = 4). The enzyme and inhibitor were pre-incubated at 37 °C for 30 min to attain equilibrium. The data were fitted to the Michaelis-Menten model to determine the $V_{max\ app}$ values and to the Lineweaver-Burk model for diagnosis of the mechanism and to determine the slope of the line at each inhibitor concentration. With the primary data, two

secondary plots were used, as recommend by Copeland (2000) [26]: a) a Dixon plot of $1/V_{max\ app}$ as a function of inhibitor concentration, for determination of the αK_i value (x intercept), b) a plot of the slopes from Lineweaver-Burk plot as a function of inhibitor concentration for determination of the K_i value (x intercept). Combining information from these two secondary plots allows determination of both inhibitor dissociation constants from a single set of experimental data [26]. For pAPA, we studied the effect of a fixed concentration of each inhibitor (5 μM) at different concentrations of the substrate (0.12, 0.25, 0.75 and 1.25 mM) for preliminary identification of the kinetic mode of inhibition.

2.7. In vivo effects of inhibitors on APN activity in a rodent model

Wistar rats (80–100 days old, 260–300 g) kept under controlled lighting conditions (light on from 07:00 to 19:00 h) and fed *ad libitum* were treated according to the "Society for Neuroscience" (USA) recommendations. BTB11079, JFD00064, and BTB07018 were dissolved in 0.9% saline just before use. The inhibitor (3 μg/g body weight, dissolved in 100 μL saline), or saline alone, was injected intraperitoneally (at 10:00 a.m.); rats were sacrificed by decapitation 1 h after injection (6 animals for each inhibitor and vehicle). Brain, intestine, liver, kidneys and pancreas were rapidly dissected, frozen on dry ice and kept at −70 °C. Membranes were prepared at 4 °C by homogenization of each organ with a Potter-Elvehjem homogenizer in 10% (w/v) buffer A. The homogenate was centrifuged at 1000 g for 15 min, the pellet re-suspended with half the amount of buffer and centrifuged again. The two supernatants were pooled, centrifuged at 12 000 g for 15 min, the pellet re-suspended in 1 M NaCl in buffer A and re-centrifuged as described above. Pellets were re-suspended in buffer A and kept at −70 °C until assayed for APN activity and protein concentration.

2.8. Data analysis

Data represent the mean ± SD values. ANOVA followed by Tukey-Kramer posthoc test was used to determine statistical significance between individual means in the *in vivo* experiment. Differences were considered significant at p < 0.05.
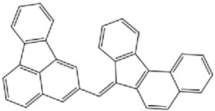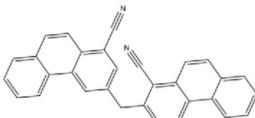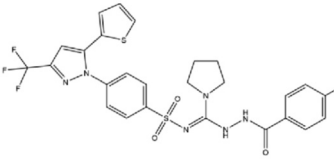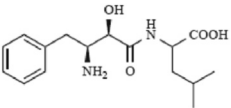
3. Results

3.1. Identification of non-competitive inhibitors of the human and porcine neutral M1 aminopeptidases

We identified more than 20 putative ligands of hAPN by screening the Maybridge Hitfinder database with the Autodock4 Zn software [16] using as target the 3D structure of the hAPN:amastatin complex (Supplementary Information Table 1). Based on the binding free energies of hAPN:Ligand complexes, we preliminary selected the four best-ranked compounds for kinetic studies with the human and porcine aminopeptidases. These putative ligands labeled as: BTB11079, JFD00064, NRB00567 and BTB07018 are hydrophobic compounds of low molecular weight (under 625 g/mol) (Table 1; Supplementary Information Table 1). However, compound NRB00567 was excluded from all the assays based on the PAINS-Remover filter analysis, due to the presence of the quinone structural moieties in its scaffold. The 2D structure of JFD00064 and BTB07018 contains hydrogen bond acceptor groups. Interestingly, the analysis of the 2D structure of BTB07018 showed two hydrogen bond donor groups (Supplementary Information Table 1 and Supplementary Information Fig. 1).

Dose-response studies were performed to identify the range of effective inhibitor concentration on the activity of pAPN and hAPN. In all the enzymatic assays bestatin was included as control. The

Table 1
Inhibition of hAPN and pAPN activities by Maybridge inhibitors and bestatin.

Inhibitor code	2D structure	MW (g/mol)	Ki (µM)		Inhibition Type
			hAPN	pAPN	
BTB11079		428.53	5.95	1.63 ($\alpha = 11.40$)	Non-competitive $\alpha > 1$
JFD00064		418.49	2.01	2.90 ($\alpha = 2.69$)	Non-competitive $\alpha > 1$
BTB07018		623.07	1.01	1.95 ($\alpha = 1.82$)	Non-competitive $\alpha > 1$
Bestatin		308.37	ND	5.59 ($\alpha = 5.97$)	Non-competitive $\alpha > 1$

substrate concentration in each assay was equivalent to the K_M values that were: 0.305 ± 0.050 mM for pAPN and 0.025 ± 0.004 mM for hAPN. A dose dependent reversible inhibition was obtained for all the inhibitors (see concave curves in Fig. 1) using a pre-incubation step of 30 min to reach equilibrium. Similar inhibition profiles were obtained using two different substrates and methods of detection. IC_{50} values were in the range of 2.29—2.95 µM for pAPN and 2.67—4.60 µM for hAPN (Fig. 1). As result of the dilution approach to test reversibility, a 10 fold drop in inhibitor concentration (to 0.1 IC_{50} values) increased the residual activity of pAPN (as fraction of the control assay) up to 0.96—0.99 of the initial rate, compared to residual activities in the range of 0.51—0.56 in standard assays (Supplementary Information Table 2).

Once the reversibility of the system was established, indicative of a specific inhibition of APN, a kinetic mechanistic approach was followed. To determine the strength and type of inhibition of the compounds against porcine aminopeptidase activity, the Michaelis-Menten model and the Lineweaver-Burk approximation were used (Fig. 2 A—D, A'-D', respectively). The details of the fitting to both mathematic models are shown in Supplementary Information Table 3. The pattern of straight lines in the double-reciprocal plots represented the signature for a typical non-competitive inhibition profile for all the inhibitors [26,27]; this implies that the inhibitors display binding affinity for both the free enzyme and the enzyme-substrate binary complex, and suggests that they do not compete with the substrate for binding to the free enzyme. Remarkably, the lines intersect above the x and y axes, at negatives values of 1/[S] and positive values of 1/v, indicating that all the inhibitors decrease the affinity of the enzyme for the substrate (signature $\alpha > 1$) (Fig. 2 A'-D') [26,27]. This mode of inhibition is also referred to as mixed inhibition, based on the effect of increasing inhibitor concentration on both V_{max} and K_M values. Similar inhibition profiles were obtained for the interaction of the compounds with the hAPN (data not shown). The secondary plots used for K_i and αK_i determination are shown in Supplementary Information Fig. 4. The K_i values vs pAPN were in the range of 1.63—5.59 µM with α values in the range of 1.82—11.40 (Table 1, Supplementary Information Table 3). Similar K_i values vs hAPN were also observed (Table 1).

3.2. Non-competitive inhibitors may target human neutral M1 aminopeptidases without Zn coordination

Chelation of zinc ions through a ZBG is the most common mode of action for inhibitors targeting aminopeptidases [13,28—30]. In this study, we identified APN inhibitors which chemical structures did not contain the classical ZBG. To figure out how these molecules inhibit human and porcine neutral aminopeptidases, we analyzed the binding mode of the inhibitors to the human APN obtained by molecular docking simulations. We observed a remarkable prevalence of hydrophobic interactions with aliphatic (Ala-351 and Ala-353), aromatic (Phe-472, Tyr-891, and Phe-896) and polar (Gln-211 and Gln-213) residues (Fig. 3). The compounds did not coordinate the zinc ion in the active site, and established few hydrophobic interactions with the metal coordinating residues His388, His392, and Glu411 (Fig. 3). We predicted that all the inhibitors bind to Tyr477, a residue involved in the stabilization of the transition state oxyanion form, through hydrophobic interactions, and that compounds BTB11079 and BTB07018 establish hydrophobic interactions with Glu389, a key residue for polarizing the water molecule that attacks the scissile peptide bond. Contrary to bestatin [2], we predicted interactions of the identified inhibitors with residues: Ser-415, Glu-418, Tyr-419, Asn-438, Asp-439 Arg-442, Asp-473, Ala-474, Asn-900, and Gln-903 (Fig. 3). Except for Gln-903, these residues have not been associated with any step of the catalysis mechanism of the aminopeptidases.

To understand the non-competitive inhibition profile, it was critical to address inhibitor interactions with residues enrolled in the substrate binding pocket and other putative subsites. Therefore, we docked the substrate in the active site of hAPN and subsequently we aligned the 3D structure of the APN:substrate complex over the APN:inhibitor complexes to generate ternary APN-
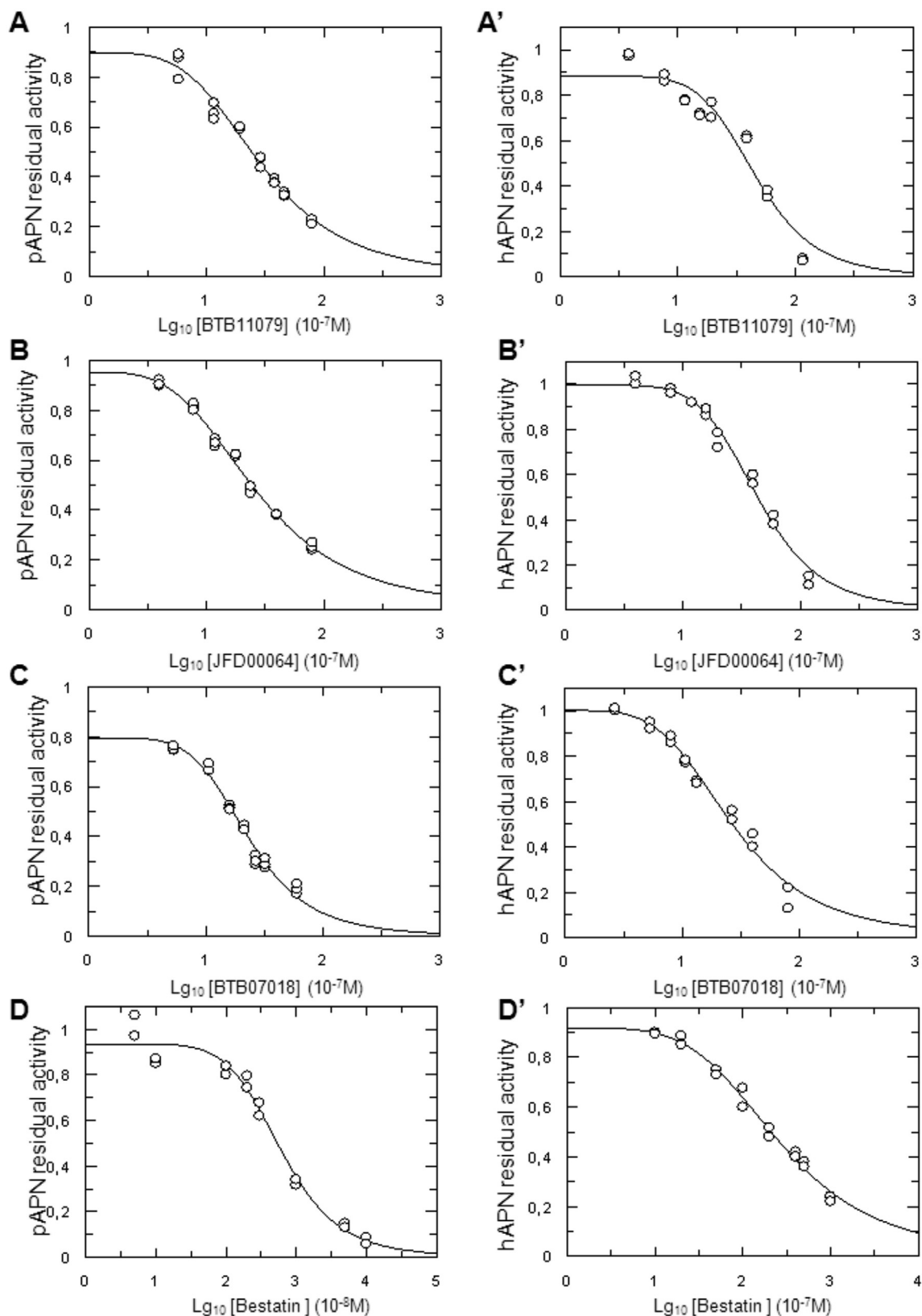
Fig. 1. The selected compounds inhibit pAPN and hAPN activities: dose-response curves. Left panels show the effect of the inhibitors vs pAPN; right panels vs hAPN. BTB11079 (A, A′), JFD00064 (B, B′), BTB07018 (C, C′) and bestatin (D, D′). The enzymes were pre-incubated with each inhibitor for 30 min to attain equilibrium. Results are mean for n = 4. The compounds inhibited both enzymes with similar IC_{50} values: IC_{50} vs pAPN: BTB11079: 2.95 ± 0.10 μM; JFD00064: 2.83 ± 0.10 μM; BTB07018: 2.29 ± 0.10 μM; bestatin: 6.13 ± 0.11 μM. IC_{50} vs hAPN: BTB11079: 4.60 ± 0.11 μM; JFD00064: 4.35 ± 0.11 μM; BTB07018: 2.67 ± 0.11 μM; bestatin: 25.7 ± 0.10 μM.
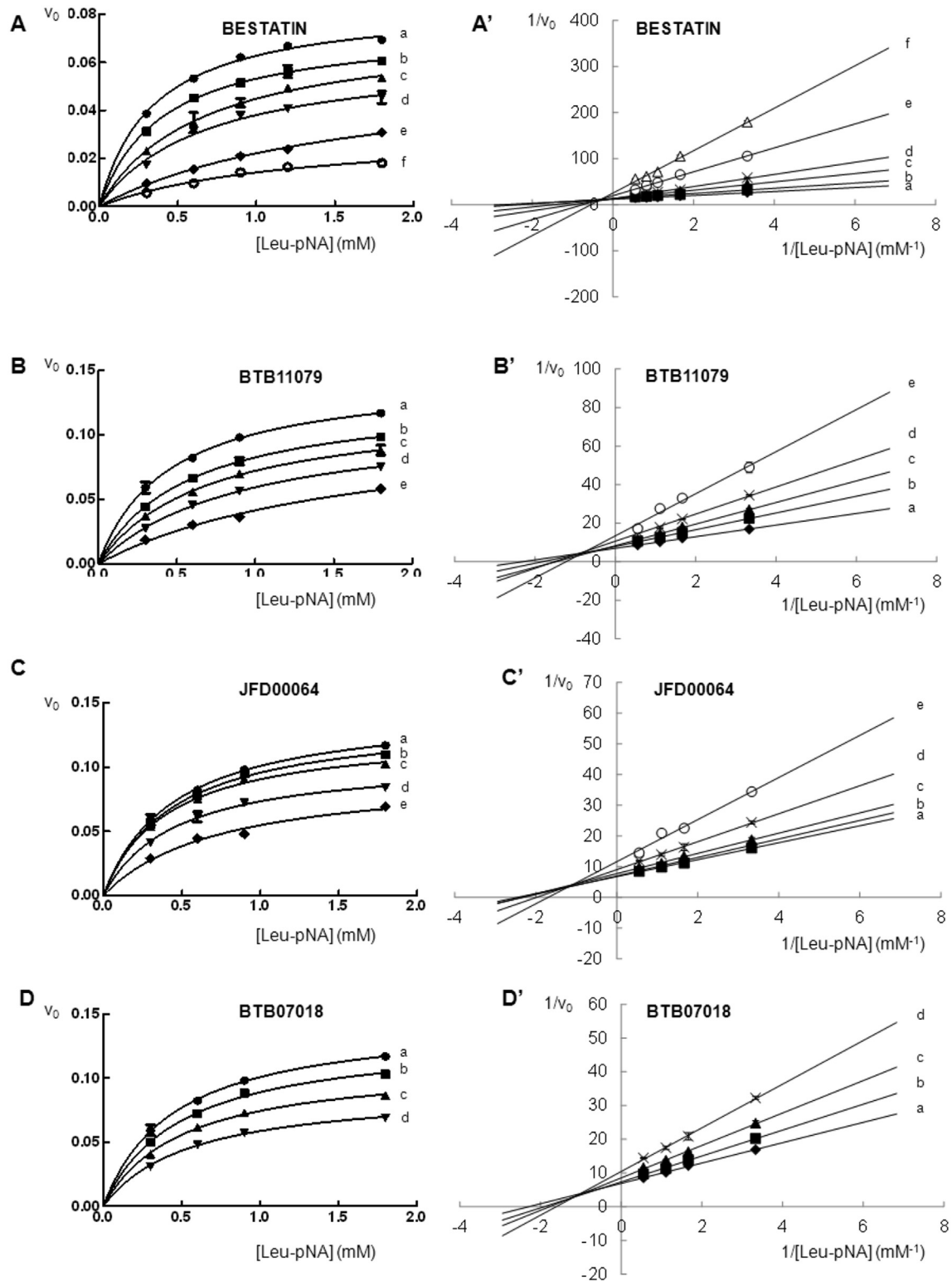
Fig. 2. Determination of the kinetic mode of action of the inhibitors vs pAPN using Michaelis-Menten model and Lineweaver-Burk plots. Left panel (A, B, C, D): non-linear regression fitting to a standard Michaelis-Menten model. Right panel (A′, B′, C′, D′): Lineweaver-Burk plot for diagnosis of inhibitor modality. Letters a-f refer to the inhibitor concentration in the assay, from the lowest to the highest. For bestatin (A): 0, 1.0, 5.0, 10.0, 30.0 and 50.0 μM. For BTB11079 (B): 0, 0.63, 1.26, 2.52 and 5.04 μM. For JFD00064 (C): 0, 0.54, 1.08, 2.16 and 4.32 μM. For BTB07018 (D): 0, 0.56, 1.12 and 2.25 μM. Results are mean ± SD for n = 4.

inhibitor-substrate complexes (Fig. 3). Remarkably, we predicted that none of the compounds interacted with all the residues belonging to the substrate binding site, leaving unoccupied spaces that allow inhibitor and substrate binding to the enzyme at the same time (Fig. 3). The analysis of the 3D structure of the enzyme-inhibitor-substrate complexes revealed that inhibitor-enzyme
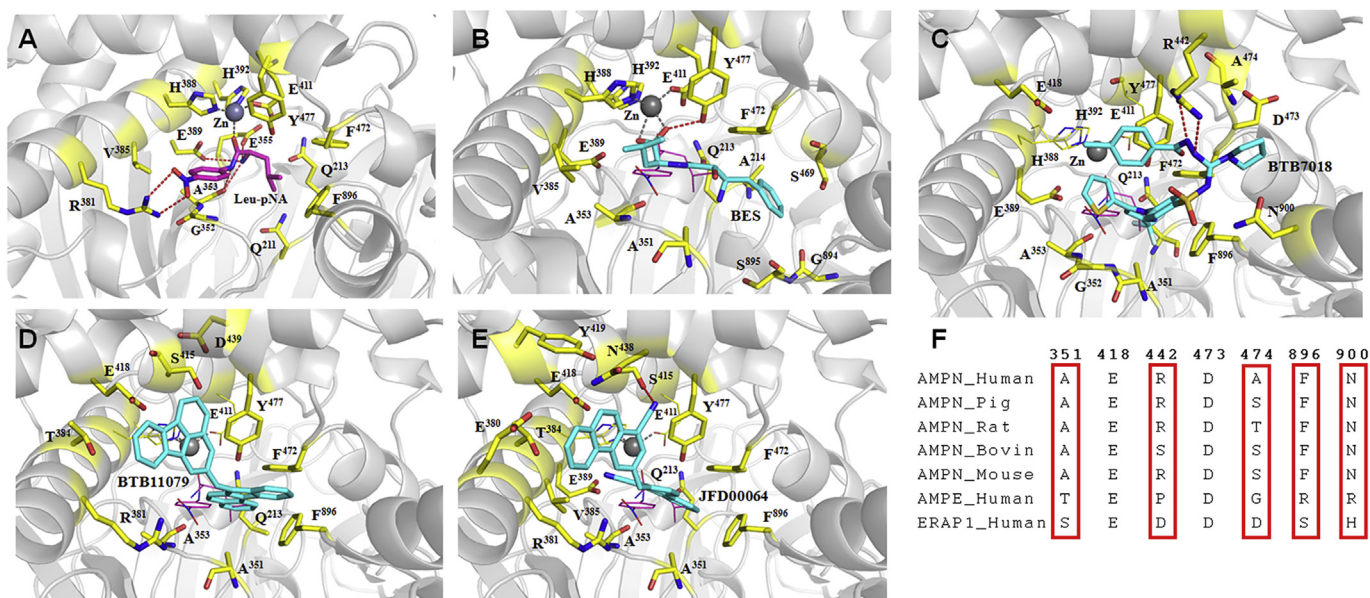
Fig. 3. Binding mode of the hAPN:ligand complexes A) hAPN:Substrate B) hAPN:Bestatin:Substrate, C) hAPN:BTB07018:Substrate, D) hAPN:BTB11079:Substrate, and E) hAPN:JFD00064:Substrate. F) Sequence analysis of contact residues among several members of the M1 family of neutral aminopeptidases homologous to the human APN. All the inhibitors and the substrate in panel A are represented as stick. For clarity the substrate is represented as lines in all the hAPN:Inhibitor:Substrate complexes. Color codes: ligand atoms: carbon in magenta, oxygen in red, sulfur in yellow, and nitrogen in blue; atoms of the protein contact residues: carbon (blue light), oxygen (red), nitrogen (blue), and the Zn atom (gray). The hydrogen bonds interactions are represented as red dotted lines and the Zn coordination as gray dotted lines. For clarity, we didn't represent the van der Waals interactions between ligands and protein contact residues. Uniprot codes: human APN (AMPN_HUMAN); they included APN from pig (AMPN_PIG), rat (AMPN_RAT) and bovine (AMPN_BOVINE) species. We also included in our analysis the human glutamyl (AMPE_Human) and endoplasmic reticulum (ERAP1_HUMAN) aminopeptidases. The specific residues of neutral aminopeptidases targeted by the inhibitors are highlighted by red rectangles.

interactions span residues comprised among the S1 and S5′ subsites, while the substrate interacts only with the S1 subsite (Fig. 3). The differences between the enzyme binding mode of the new inhibitors and of the substrate explained the non-competitive inhibition profile. Thus, we predicted that compound BTB07018 established interactions with residues: Ala-351, Glu-418, Arg-442, Asp-473, Ala-474, Phe-896 and Asn-900, which were not shared by the substrate.

To obtain preliminary information on specificity, we tested the inhibitors on pAPA, another well-established therapeutic target in the M1 family [13]. We observed that BTB11079, JFD00064, and BTB07018 inhibited pAPA in a dose-dependent manner (Supplementary Information Fig. 5), in a range of concentration similar to that for pAPN (IC$_{50}$ values: BTB11079: 3.88 ± 0.11 μM, JFD00064: 1.82 ± 0.11 μM, BTB07018: 4.74 ± 0.10 μM). However, the pattern of straight lines in the double-reciprocal plots, obtained as a result of a preliminary study at a fixed concentration of each inhibitor and increasing concentration of the substrate L-Glu-pNA, indicated the signature for a competitive mode of inhibition (Supplementary Information Fig. 5). The analysis of the sequence of other aminopeptidases of the M1 family suggests that targeting residues: Ala-351, Arg-442, Ala-474, Phe-896 and Asn-900 should improve the selectivity of neutral aminopeptidase inhibitors (Fig. 3).

3.3. In vivo effects of the non-competitive inhibitors of neutral M1 aminopeptidase activity in rat organs

The effect of the inhibitors on the activity of APN in various tissues of rats was evaluated *in vivo*. We chose this animal model due to the strong conservation of inhibitor interacting residues within mammalian neutral aminopeptidases (Supplementary Information Fig. 6). The intraperitoneal injection of 3 μg /g b.w. of either compound BTB11079, JFD00064 or BTB07018/g did not

induce any mortality or change in rat spontaneous behavior, compared to the vehicle group (not shown). Injection of JFD00064 or BTB07018 decreased APN activity in brain, liver, and kidney 60 min later, compared to the control group (saline injected animals). Compound JFD00064 also inhibited the APN activity in the pancreas (Fig. 4).

4. Discussion

Aminopeptidase N is a transmembrane protease present in a wide variety of human tissues and cell types (endothelial, epithelial, fibroblast, leukocyte). APN expression is dysregulated in inflammatory diseases as well as in solid and hematologic tumors [12]. Therefore, inhibitors of APN may be effective against cancer and inflammation [12,31,32]. Chelating zinc ions through a ZBG is the most common mode of action of neutral aminopeptidase inhibitors [13,28–30,33–38]. Most of these inhibitors display a competitive inhibition mode of action. Here, we identified three non-competitive inhibitors ($\alpha > 1$) of human and porcine neutral aminopeptidases; these ligands do not contain a ZBG in their 3D structure. The K$_i$ values of these new compounds were similar to those reported for natural APN inhibitors [12,29]. Molecular docking simulations predicted that the inhibitors bind to a site distinct from that occupied by the substrate in the human APN active site (Fig. 3). This is consistent with the non-competitive inhibition profile obtained in the kinetic assays. The analysis of hAPN:Inhibitor complexes showed that interactions span from S1 to S5′ subsites, without Zn ion coordination. This uncommon mechanism of inhibition is similar to that described for compound MMV666023, an inhibitor of the neutral M1 aminopeptidase of *Plasmodium falciparum* [39]. The newly identified inhibitors share with compound MMV666023 a high hydrophobicity and a lack of typical ZBG [39]. The lack of ZBG may diminish inhibitor interactions with other metalloenzymes, and may improve pharmacokinetics and oral
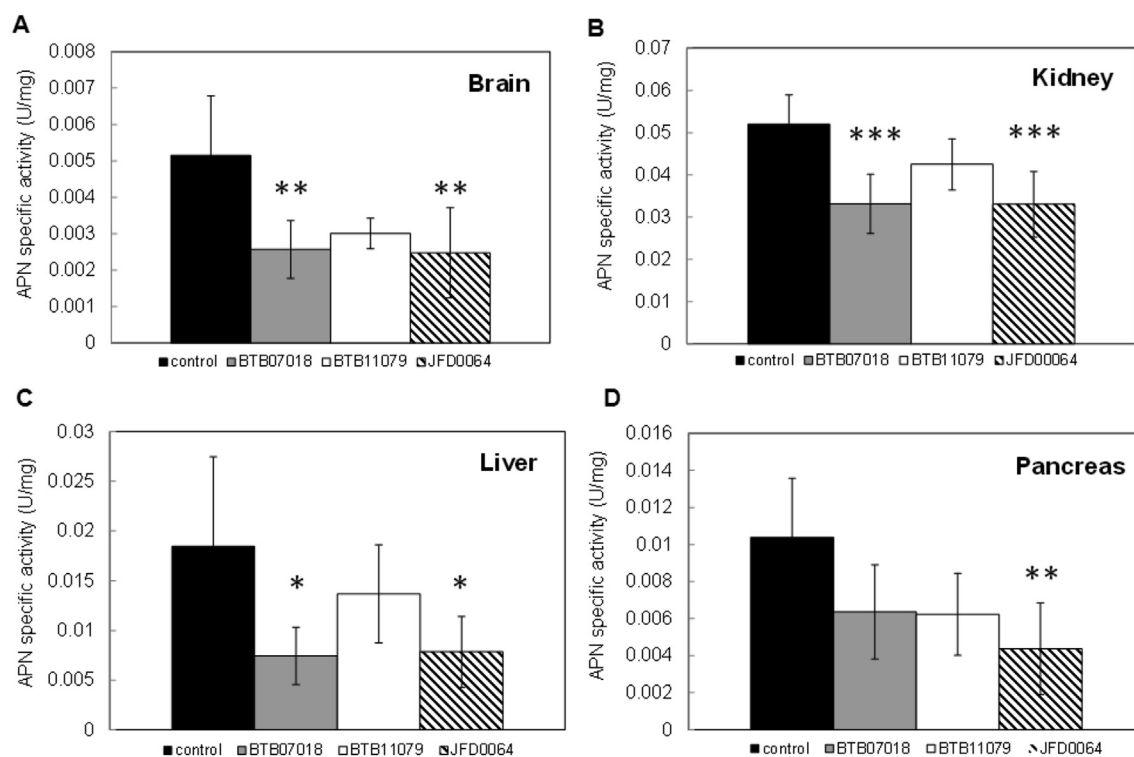
Fig. 4. *In vivo* **effect of inhibitors on APN activity in (A) brain, (B) kidney, (C) liver, and (D) pancreas of adult male rats**. Animals were inoculated with a single injection of saline (vehicle) or inhibitor (3 μg/g b.w. of BTB11079, JFD00064 or BTB07018), and sacrificed by decapitation 60 min later. Tissues were rapidly dissected, frozen on dry ice and kept at −70 °C until preparation of membranes for evaluation of APN activity as described in Materials and Methods. Data are mean ± SD (n = 6). ANOVA data: brain (F = 6.673, P < 0.001), kidney (F = 10.061, P < 0.001), liver (F = 5.235, P < 0.05), pancreas (F = 5.549, P < 0.001). Tukey-Kramer posthoc test: *: p < 0.05; **: p < 0.01; ***: p < 0.001.

bioavailability of APN inhibitors [39]. Additional experiments, including site-directed mutagenesis and crystallography studies, are needed to confirm the binding mode of the hAPN:Inhibitor complexes.

To check the selectivity of the inhibitor we tested its activity over porcine APA. APN and APA form the same interactions with the main chain of the N-terminal residue (P1 residue) of their ligands, suggesting that the two enzymes share a common catalytic mechanism despite their modest sequence similarity [2,40]. However, the S1 pocket that accommodates the P1 side chain of ligands differs markedly between APN and APA, consistent with the different substrate specificities of the two enzymes. Residues Phe-896 and Ala-351 of the S1 pocket of APN favor the accommodation of bulky hydrophobic side chains [2]. Conversely, the S1 pocket of APA is well suited to accommodate the side chains of acidic residues; the carboxylate side chain of bound glutamate forms a strong salt bridge with Arg-887 and a hydrogen bond with Thr-356. These energetically favorable interactions are consistent with high APA activity on substrates with a P1 glutamate [40]. Therefore, we did not expect selectivity of the identified inhibitors for APN over APA because we predicted these ligands target several conserved residues. Preliminary kinetics experiments confirmed that the new compounds also inhibited pAPA with IC_{50} values similar to those detected for pAPN. However, BTB11079, JFD00064, and BTB07018 displayed a competitive inhibition mode that differed from that vs pAPN. This may result from an accommodation of the inhibitors at the active site of pAPA that differs from the binding mode predicted for APN. Additional experiments should clarify the selectivity of the newly identified inhibitors against other aminopeptidases of the M1 family, and may identify dual inhibitions of biomedical relevance [13]. Based on the sequence and structural analyses, we predicted that targeting the APN residues Ala-351, Arg-442, Ala-

474, Phe-896 and Asn-900 might be useful for improving the selectivity of the identified inhibitors.

The inhibition of APN activity by two of the compounds in rat brain, kidney, or liver suggests their rapid absorption and wide biodistribution. This finding is relevant due to the implication of APN in physio- and patho-physiological processes in these tissues [41–46]. Many hydrophobic drugs reversibly bind to Site 1 of human serum albumin (HSA), an association that improves the pharmacokinetics properties of therapeutic compounds [47]. Since mammalian serum albumins share more than 70% of sequence identity and have similar functions [48], the effective delivery of JFD00064 and BTB07018 to rat tissues may have been facilitated by their reversible binding to rat serum albumin hydrophobic sites. Moreover, HSA delivery systems have been extensively studied for treating brain disease since HSA can pass through the blood brain barrier [48]; interestingly, compounds JFD00064 and BTB07018 inhibited APN activity in the brain of rats, indicating these molecules crossed the blood-brain barrier. Further experiments are needed to confirm the interaction of these ligands with serum albumin.

5. Conclusion

We have identified three non-competitive inhibitors of the human and porcine APN with Ki values in the μM range, by combining virtual screening and kinetic assays. Molecular docking simulations suggest these novel inhibitors block APN activity by an alternative mechanism to Zn coordination. Of note, these compounds also inhibited the porcine aminopeptidase A (pAPA) by a competitive inhibition mode. This indicated differences in the binding mode of these compounds with APN and APA. Based on sequence and structural analyses we predict that targeting human APN residues:

A351, R442, A474, F896 and N900 may lead to the design of more selective APN inhibitors. Remarkably, compounds BTB07018 and JFD00064 inhibited APN activity in the brain, liver and kidney of rats indicating a good bio-distribution *in vivo*. Compound BTB07018 seemed to be the most promising lead among the identified inhibitors due to its cLogP <4. This work reinforces the recent idea of designing novel APN inhibitors based on lead compounds without ZBG.

Notes

The authors declare no competing financial interest.

Acknowledgments

Appendix A. Supplementary data

Supplementary data related to this article can be found at https://doi.org/10.1016/j.biochi.2017.09.015.

References

[1] P. Mina-Osorio, The moonlighting enzyme CD13: old and new functions to target, Trends Mol. Med. 14 (2008) 361—371.
[2] A.H.M. Wong, D. Zhou, J.M. Rini, The x-ray crystal structure of human aminopeptidase N reveals a novel dimer and the basis for peptide processing, J. Biol. Chem. 287 (2012) 36804—36813.
[3] W.N. Lipscomb, N. Strater, Recent advances in zinc enzymology, Chem. Rev. 96 (1996) 2375—2434.
[4] A. Addlagatta, L. Gay, B.W. Matthews, Structure of aminopeptidase N from Escherichia coli suggests a compartmentalized, gated active site, Proc. Natl. Acad. Sci. U. S. A. 103 (2006) 13339—13344.
[5] K. Ito, Y. Nakajima, Y. Onohara, M. Takeo, K. Nakashima, F. Matsubara, T. Ito, T. Yoshimoto, Crystal structure of aminopeptidase N (proteobacteria alanyl aminopeptidase) from Escherichia coli and conformational change of methionine 260 involved in substrate recognition, J. Biol. Chem. 281 (2006) 33664—33676.
[6] S. McGowan, C.J. Porter, J. Lowther, C.M. Stack, S.J. Golding, T.S. Skinner-Adams, K.R. Trenholme, F. Teuscher, S.M. Donnelly, J. Grembecka, A. Mucha, P. Kafarski, R. Degori, A.M. Buckle, D.L. Gardiner, J.C. Whisstock, J.P. Dalton, Structural basis for the inhibition of the essential Plasmodium falciparum M1 neutral aminopeptidase, Proc. Natl. Acad. Sci. U. S. A. 106 (2009) 2537—2542.
[7] M. Konig, A.M. Zimmer, H. Steiner, P.V. Holmes, J.N. Crawley, M.J. Brownstein, A. Zimmer, Pain responses, anxiety and aggression in mice deficient in pre-proenkephalin, Nature 383 (1996) 535—538.
[8] R.S. Danziger, Aminopeptidase N in arterial hypertension, Heart Fail. Rev. 13 (2008) 293—298.
[9] P. Datar, S. Srivastava, E. Coutinho, G. Govil, Substance P: structure, function, and therapeutics, Curr. Top. Med. Chem. 4 (2004) 75—103.
[10] Y. Xu, D. Wellner, D.A. Scheinberg, Substance P and bradykinin are natural inhibitors of CD13/aminopeptidase N, Biochem. Biophys. Res. Commun. 208 (1995) 664—674.
[11] B. Bauvois, Transmembrane proteases in cell growth and invasion: new contributors to angiogenesis? Oncogene 23 (2004) 317—329.
[12] B. Bauvois, D. Dauzonne, Aminopeptidase-N/CD13 (EC 3.4.11.2) inhibitors: chemistry, biological evaluations, and therapeutic prospects, Med. Res. Rev. 26 (2006) 88—130.
[13] N. Drinkwater, J. Lee, W. Yang, T.R. Malcolm, S. McGowan, M1 aminopeptidases as drug targets: broad applications or therapeutic niche? FEBS J. 284 (2017) 1473—1488.
[14] N.M. O'Boyle, M. Banck, C.A. James, C. Morley, T. Vandermeersch, G.R. Hutchison, Open Babel: an open chemical toolbox, J. Cheminformatics 3 (2011) 1—14.
[15] D. Santos-Martins, S. Forli, M.J. Ramos, A.J. Olson, AutoDock4Zn: an improved AutoDock force field for small-molecule docking to zinc metalloproteins,

[16] J. Chem. Inf. Model. 54 (2014) 2371—2379.
G.M. Morris, R. Huey, W. Lindstrom, M.F. Sanner, R.K. Belew, D.S. Goodsell, A.J. Olson, AutoDock4 and AutoDockTools4: automated docking with selective receptor flexibility, J. Comput. Chem. 30 (2009) 2785—2791.
[17] J.B. Baell, G.A. Holloway, New substructure filters for removal of pan assay interference compounds (PAINS) from screening libraries and for their exclusion in bioassays, J. Med. Chem. 53 (2010) 2719—2740.
[18] A.C. Wallace, R.A. Laskowski, J.M. Thornton, LIGPLOT: a program to generate schematic diagrams of protein-ligand interactions, Protein Eng. 8 (1995) 127—134.
[19] M.S. Madhusudhan, B.M. Webb, M.A. Marti-Renom, N. Eswar, A. Sali, Alignment of multiple protein structures based on sequence and structure features, Protein Eng. Des. Sel. 22 (2009) 569—574.
[20] A. Sali, T.L. Blundell, Comparative protein modeling by satisfaction of spatial restraints, J. Mol. Biol. 234 (1993) 779—815.
[21] J.D. Thompson, D.G. Higgins, T.J. Gibson, CLUSTAL W: improving the sensitivity of progressive multiple sequence alignment through sequence weighting, position-specific gap penalties and weight matrix choice, Nucleic Acids Res. 22 (1994) 4673—4680.
[22] N. Galtier, M. Gouy, C. Gautier, SEAVIEW and PHYLO_WIN: two graphic tools for sequence alignment and molecular phylogeny, Comput. Appl. Biosci. 6 (1996) 543—548.
[23] S. Tieku, N.M. Hooper, Inhibition of aminopeptidases N, A and W. A re-evaluation of the actions of bestatin and inhibitors of angiotensin converting enzyme, Biochem. Pharmacol. 44 (1992) 1725—1730.
[24] I. Florent, Z. Derhy, M. Allary, M. Monsigny, R. Mayer, J. Schrevel, A Plasmodium falciparum aminopeptidase gene belonging to the M1 family of zinc-metallopeptidases is expressed in erythrocytic stages, Mol. Biochem. Parasitol. 97 (1998) 149—160.
[25] M. Allary, J. Schrevel, I. Florent, Properties, stage-dependent expression and localization of Plasmodium falciparum M1 family zinc-aminopeptidase, Parasitology 125 (2002) 1—10.
[26] R.A. Copeland, Enzymes: a Practical Introduction to Structure, Mechanism, and Data Analysis., Enzymes, Wiley-VCH, Inc., New York, 2000, pp. 266—304.
[27] R.A. Copeland, in: Evaluation of Enzyme Inhibitors in Drug Discovery: a Guide for Medicinal Chemists and Pharmacologists, second ed., John Wiley & Sons, Inc., Hoboken, New Jersey, 2013.
[28] N.D. Rawlings, A.J. Barrett, R. Finn, Twenty years of the MEROPS database of proteolytic enzymes, their substrates and inhibitors, Nucleic Acids Res. 44 (2016) D343—D350.
[29] A. Mucha, M. Drag, J.P. Dalton, P. Kafarski, Metallo-aminopeptidase inhibitors, Biochimie 92 (2010) 1509—1529.
[30] Q. Zhang, J. Wang, H. Zhang, D. Zhao, Z. Zhang, S. Zhang, Expression and clinical significance of aminopeptidase N/CD13 in non-small cell lung cancer, J. Cancer Res. Ther. 11 (2015) 223—228.
[31] C. Schmitt, M. Voegelin, A. Marin, M. Schmitt, F. Schegg, P. Henon, D. Guenot, C. Tarnus, Selective aminopeptidase-N (CD13) inhibitors with relevance to cancer chemotherapy, Bioorg Med. Chem. 21 (2013) 2135—2144.
[32] C. Ma, J. Cao, X. Liang, Y. Huang, P. Wu, Y. Li, W. Xu, Y. Zhang, Novel leucine ureido derivatives as aminopeptidase N inhibitors. Design, synthesis and activity evaluation, Eur. J. Med. Chem. 108 (2016) 21—27.
[33] H. Pan, K. Yang, J. Zhang, Y. Xu, Y. Jiang, Y. Yuan, X. Zhang, W. Xu, Design, synthesis and biological evaluation of novel L-isoserine tripeptide derivatives as aminopeptidase N inhibitors, J. Enzyme Inhib. Med. Chem. 28 (2013) 717—726.
[34] Q. Li, H. Fang, X. Wang, G. Hu, Q. Wang, W. Xu, Novel potent 2,5-pyrrolidinedione peptidomimetics as aminopeptidase N inhibitors. Design, synthesis and activity evaluation, Bioorg. Med. Chem. Lett. 22 (2012) 850—853.
[35] K. Jin, X. Zhang, C. Ma, Y. Xu, Y. Yuan, W. Xu, Novel indoline-2,3-dione derivatives as inhibitors of aminopeptidase N (APN), Bioorg. Med. Chem. 21 (2013) 2663—2670.
[36] S. Albrecht, M. Al-Lakkis-Wehbe, A. Orsini, A. Defoin, P. Pale, E. Salomon, C. Tarnus, J.-M. Weibel, Amino-benzosuberone: a novel warhead for selective inhibition of human aminopeptidase-N/CD13, Bioorg. Med. Chem. 19 (2011) 1434—1449.
[37] G. Revelant, M. Al-Lakkis-Wehbe, M. Schmitt, S. Alavi, C. Schmitt, L. Roux, M. Al-Masri, N. Schifano-Faux, C. Maiereanu, C. Tarnus, S. Albrecht, Exploring S1 plasticity and probing S1' subsite of mammalian aminopeptidase N/CD13 with highly potent and selective aminobenzosuberone inhibitors, Bioorg Med. Chem. 23 (2015) 3192—3207.
[38] E. Weglarz-Tomczak, L. Berlicki, M. Pawelczak, B. Nocek, A. Joachimiak, A. Mucha, A structural insight into the P1S1 binding mode of diaminoethylphosphonic and phosphinic acids, selective inhibitors of alanine aminopeptidases, Eur. J. Med. Chem. 117 (2016) 187—196.
[39] A. Paiardini, R.S. Bamert, K. Kannan-Sivaraman, N. Drinkwater, S.N. Mistry, P.J. Scammells, S. McGowan, Screening the medicines for malaria venture "malaria box" against the Plasmodium falciparum aminopeptidases, M1, M17 and M18, PLoS One 10 (2015) e0115859.
[40] Y. Yang, C. Liu, Y.L. Lin, F. Li, Structural insights into central hypertension regulation by human aminopeptidase A, J. Biol. Chem. 288 (2013) 25638—25645.
[41] E. Bonnard, H. Poras, X. Nadal, R. Maldonado, M.C. Fournie-Zaluski, B.P. Roques, Long-lasting oral analgesic effects of N-protected aminophosphinic dual ENKephalinase inhibitors (DENKIs) in peripherally controlled

pain, Pharmacol. Res. Perspect. 3 (2015) e00116.

[42] M. Wickstrom, R. Larsson, P. Nygren, J. Gullbo, Aminopeptidase N (CD13) as a target for cancer chemotherapy, Cancer Sci. 102 (2011) 501—508.

[43] H. Poras, E. Bonnard, E. Dange, M.C. Fournie-Zaluski, B.P. Roques, New orally active dual enkephalinase inhibitors (DENKIs) for central and peripheral pain treatment, J. Med. Chem. 57 (2014) 5748—5763.

[44] N. Haraguchi, H. Ishii, K. Mimori, F. Tanaka, M. Ohkuma, H.M. Kim, H. Akita, D. Takiuchi, H. Hatano, H. Nagano, G.F. Barnard, Y. Doki, M. Mori, CD13 is a therapeutic target in human liver cancer stem cells, J. Clin. Investig. 120 (2010) 3326—3339.

[45] G. Larrinaga, L. Blanco, B. Sanz, I. Perez, J. Gil, M. Unda, L. Andres, L. Casis, J.I. Lopez, The impact of peptidase activity on clear cell renal cell carcinoma survival, American journal of physiology, Ren. Physiol. 303 (2012) F1584—F1591.

[46] S. Saida, K. Watanabe, I. Kato, H. Fujino, K. Umeda, S. Okamoto, S. Uemoto, T. Hishiki, H. Yoshida, S. Tanaka, S. Adachi, A. Niwa, T. Nakahata, T. Heike, Prognostic significance of aminopeptidase-N (CD13) in hepatoblastoma, Pediatr. Int. Off. J. Jpn. Pediatr. Soc. 57 (2015) 558—566.

[47] F. Yang, Y. Zhang, H. Liang, Interactive association of drugs binding to human serum albumin, Int. J. Mol. Sci. 15 (2014) 3580—3595.

[48] D.C. Carter, J.X. Ho, Structure of serum albumin, Adv. Protein Chem. 45 (1994) 153—203.